JOURNAL OF MATERIALS SCIENCE 15 (1980) 2282–2295

Proof testing of ceramics

Part 2 *Theory*

E. R. FULLER Jr, S. M. WIEDERHORN
National Bureau of Standards, Washington, D.C. 20234, U.S.A.

J. E. RITTER Jr, P. B. OATES
Mechanical Engineering Department, University of Massachusetts, Amherst, Massachusetts 01003, U.S.A.

Theoretical estimates are made of strength distributions after proof testing. Assuming that the crack velocity can be expressed as a power function of the stress intensity factor, $v = AK_I^n$, an analysis of the amount of strength loss during a load cycle is presented for single-region crack propagation. For multi-region crack propagation, a numerical analysis is used to describe strength loss. In both analyses, the effects of environment and loading rate are studied. For single region crack propagation, the strength after proof testing can be represented by two Weibull curves: one with a slope of m at high cumulative failure probability levels; the other with a slope of $n - 2$ at low failure probability levels. Truncation of the strength distribution always occurs as the result of proof testing; the truncation strength depends on the rate of unloading. Multi-region crack propagation results in a more complicated strength distribution after proof testing. Bimodal strength distributions occur as a consequence of region II type crack growth (i.e. $n = 0$). Theoretical results confirm experimental findings that proof tests must be conducted at rapid unloading rates and with good environmental control to be effective.

1. Introduction

The first part of this two part study presented the results of an experimental investigation of the effect of proof testing on the strength of a set of soda-lime–silica glass microscopic slides. Effects of stress cycle and test environment were investigated. Agreement between experimental results and theoretical predictions of strength distributions after proof testing were obtained when proof tests were conducted in inert environments, or when rapid rates of loading and short hold times were used in the proof tests. By contrast, when water was present in the environment and when slow rates of loading were used, strength distributions were obtained after proof testing that were not consistent with simple theoretical predictions. At the conclusion of Part I of this study, we noted that the lack of agreement between theory and experiment may be a consequence of the complex crack growth behaviour associated with crack motion in moist gaseous environments. We also suggested that additional theoretical work can be conducted to explore the possibility of complex crack growth effects on strength distributions. The second part of this study explores this possibility.

In part II of this paper the effect of complex crack growth behaviour on the strength distribution after proof testing is explored by the use of a modified fracture mechanics approach. Although fracture mechanics is used as a basis for understanding proof testing, strength degradation is discussed in terms of component strength and applied stress, a modification which permits the process of strength degradation to be illustrated graphically in a relatively simple manner. Because this approach is new, a review of the earlier literature is presented to achieve a uniform and comprehensive picture of the subject. Strength degradation resulting from simple crack growth behaviour (i.e. one region crack growth) is treated analytically, while complex crack growth behaviour is treated numerically. This study illustrates

0022–2461/80/092282–14$03.40/0

the types of strength distribution curves to be expected from a population of test specimens after they have been proof tested. The complex stress distributions reported in Part I of this paper for soda-lime–silica glass are supported by the results obtained in this part of the paper. The importance of environmental control and rapid unloading during a proof test is also confirmed.

2. Strength and crack growth behaviour

The strength of ceramics is determined by the presence of small, so-called Griffith cracks in the surface. When stresses reach a critical value, crack propagation occurs and ceramics fail by brittle fracture. The level of stress required for crack propagation depends on the test environment. Crack growth usually occurs more easily in the presence of water. The effect of water on crack growth has been used to explain the well-known phenomenon of static fatigue, or delayed failure, which is a stress enhanced reaction in which water in the environment behaves as the stress corrosion agent [1].

The advent of fracture mechanics provided a method of developing deeper insight into crack growth processes in ceramic materials [2]. Fracture mechanics also offers the possibility of relating fundamental crack-growth data to strength data, so that techniques of assuring the reliability of structural materials can be developed [3]. Data obtained on ceramic materials by fracture mechanics techniques provide a relation between the crack growth velocity, v, and the driving force for fracture, the stress intensity factor, K_I. In soda-lime–silica glass, the crack velocity is dependent on both the applied stress intensity factor, K_I, and on the amount of water in the environment. The three regions of crack growth (shown schematically in Fig. 1) depend on the amount of water in the environment and the stress intensity level at the crack tip. Regions I and II result from a stress corrosion reaction between glass and water. Region I represents reaction rate limited stress-corrosion cracking; Region II represents transport rate limited stress-corrosion cracking. Region III represents environment independent fracture that depends only on the structure of the glass, and is not observed for all glass compositions. The scientific significance of this type of data has been discussed at length elsewhere, and will not be repeated here [4]. For purposes of the present paper, this type of data can be used to calculate the fracture strength of glass or other ceramic materials after they have been subjected to a proof test.

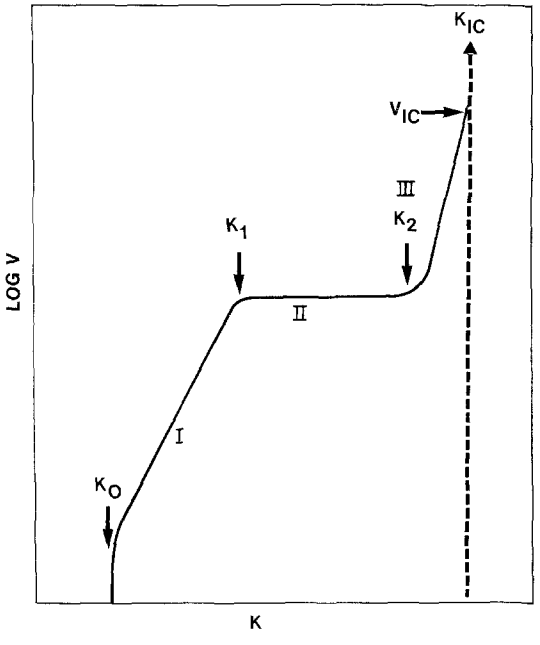

Figure 1 Dependence of crack velocity on applied stress intensity factor. Schematic diagram of crack velocity data indicating three regions of crack growth. Boundaries of these three regions are given by specific values of K_I (K_0, K_1, K_2, K_{IC}) and by a critical value of the crack velocity (V_{IC}).

Crack propagation data can be used to estimate the amount of crack growth occurring in a component that is subjected to an applied stress. Given an initial measure of the crack length, the change in crack length can be estimated from the applied load, and a functional relation between the crack velocity, v, and the stress intensity factor, K_I [i.e. $v = v(K_I)$]. For a uniform applied stress, σ, and a crack length a, K_I is given by

$$K_I = \sigma Y \sqrt{a}, \qquad (1)$$

where Y is a geometric constant. If the relation between v and K_I has the form $v = AK_I^n$, then crack growth during a stress cycle can be determined analytically and the strength of a component after a random stress cycle can be obtained. If the relation between v and K_I does not have a simple form (Fig. 1) then the strength of a component after a random stress cycle can be obtained numerically. In either case, failure occurs during the stress cycle when the stress intensity factor reaches a critical value, K_{IC}, for rapid fracture.

Quantitative estimates of the amount of crack

growth during a stress cycle can be used to evaluate the strength of a component at any point in the cycle. The fracture strength, S, at any time during the cycle can be defined in terms of the crack length, a, and the critical stress intensity factor K_{IC}, from Equation 1*

$$S = K_{IC}/Y\sqrt{a}. \quad (2)$$

If the stress, σ, equals the strength, S, at any point in the cycle, then $K_I = K_{IC}$, and failure occurs. By evaluating the effect of a stress cycle on strength, it is possible to calculate theoretical Weibull probability curves, which can then be compared with experimental ones obtained from proof test studies. Furthermore, by using a numerical procedure to evaluate the strength after a load cycle, the effect of multi-region crack propagation can be taken into account.

The strength degradation that occurs during a stress cycle can be represented by a relatively simple diagram on which are plotted simultaneously the strength of a component and the applied stress at any time during a stress cycle. Fig. 2a gives a schematic representation of a strength degradation diagram which is based on the assumption that only one region of crack growth contributes to reduction of component strength. The diagram represents a typical proof test cycle. The applied stress on the diagram is represented by the curve labelled σ which consists of three straight lines: one line representing a constant rate of stress increase during the stress cycle; the second, a horizontal line representing a hold time during the proof test; the third line representing the stress reduction as the proof test cycle is completed. Although the diagram shown in Fig. 2a is for a simple proof test cycle, any stress cycle can be represented in a similar way.

The strength of components during a stress cycle is illustrated in Fig. 2a by curves labelled, S_1, S_2 and S_3. Each of these curves represents components having different initial strengths (i.e. strengths before the start of the proof test). As the stress level in Fig. 2a is increased (curve σ), cracks present in specimens increase in size, resulting in a gradual decrease in strength. Strength degradation occurs most rapidly as the stress, σ, approaches the strength of the specimen. For specimens with initial strengths, S_1, much greater than the maximum applied stress, little strength degradation occurs during the load cycle. However, when the initial strength, S_2, is less than or approximately equal to the maximum applied stress, the specimen breaks during the test, and the breaking stress is less than that which would have

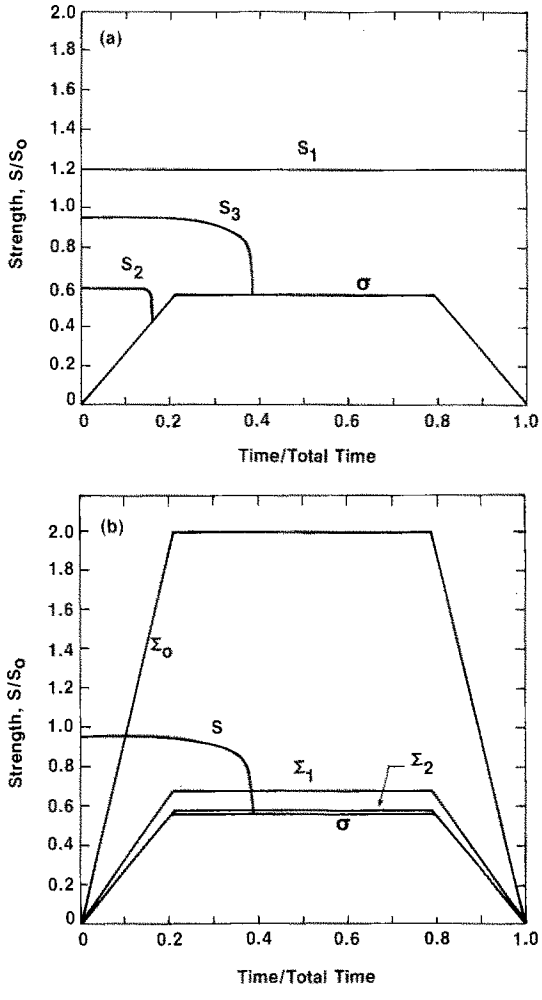

Figure 2 Schematic diagram of strength degradation maps for soda-lime–silica glass. (a) Single region crack growth. Curve labeled σ gives the applied stress as a function of time. Curves labeled S_1, S_2, S_3 give the strength as a function of time starting at different initial strength levels. (b) Three regions of crack growth (as in Fig. 1). Curves labeled Σ_0, Σ_1, Σ_2 and σ in this figure correspond to K_0, K_1, K_2 and K_{IC} of Fig. 1. The curve labeled S gives the strength degradation as a function of time.

*As defined in Equation 2, the strength is simply related to the length of the critical flaw that causes failure. In operational terms, S is the inert strength at any point of the stress cycle. It is the breaking stress that would be measured if the component could be loaded to failure in such a way that subcritical crack growth did not occur at all during the strength test.

been measured in the absence of crack growth. Breakage during the proof test can also occur when the initial strength, S_3, is greater than the maximum applied stress provided sufficient crack growth occurs during the stress cycle.

The effect of multi-region crack propagation can also be represented on this type of diagram. The lines, labelled Σ_0, Σ_1 and Σ_2 in Fig. 2b, represent the strength of components at the boundaries that separate the different regions of crack propagation (Fig. 1). For a given applied stress, these boundaries define the range of strengths that lie within each region of crack growth. The position of the boundary lines in Fig. 2b can be evaluated from the values of K_I in Fig. 1 that define the limits of each region of crack growth (i.e. K_0, K_1, K_2). For example, the curve Σ_1, that corresponds to the boundary between regions I and II in Fig. 1, $K_I = K_1$, is given in Fig. 2b by $\Sigma_1 = \sigma(K_{IC}/K_1)$, which is obtained from Equations 1 and 2 by setting $K_I = K_1$ and $S = \Sigma_1$. Thus, the boundary lines in Fig. 2b are proportional to σ, and since the proportionally constant, K_{IC}/K_1, is greater than 1, Σ_1 is greater than the applied stress, σ. In a similar way, the boundary line for K_0 is given by $\Sigma_0 = \sigma(K_{IC}/K_0)$ and that for K_2 is given by $\Sigma_2 = \sigma(K_{IC}/K_2)$.

During a proof test cycle, the value of the stress intensity factor at the most severe flaw crosses from one region of crack propagation to the next in Fig. 1 as the crack gets longer. At the same time the strength goes from one region of crack growth to the next each time the curve in Fig. 2b marked S crosses the boundary lines. At each boundary, both the slope and value of the strength curve are continuous.* Again, fracture occurs spontaneously when the strength curve touches the stress cycle boundary (i.e. when $\sigma = S$). In later sections of the paper, specific examples of these diagrams will be given.

3. Single region crack propagation

To understand the types of curves obtained on strength degradation maps, it is worth exploring single-region crack propagation. An exploration of this simple case is also useful for quantifying the basic types of curves that are to be expected in failure distributions and strength histograms. Some of the subject matter presented here has been discussed earlier, [5–11], but the treatment presented here is somewhat simplified and the results are more complete. As will be shown, this simplification is the result of considering subcritical crack growth from the point of view of strength degradation rather than crack length. New insight into the strength degradation process is obtained by this approach.

For single-region crack propagation, an analytical solution can be obtained and used to plot strength degradation diagrams, Weibull diagrams and strength histograms. In later sections of the paper, examples of such diagrams will be presented for a variety of crack propagation environments. These diagrams will be used both as a means of evaluating the effect of stressing rate and stress cycle on strength and as basis for comparison with more complex multi-region crack propagation behaviour.

The rate of strength degradation can be obtained by differentiating Equation 2 with respect to time

$$\begin{aligned} dS/dt &= -(K_{IC}/2Y)a^{-3/2}(da/dt) \\ &= -(Y^2/2K_{IC}^2)S^3v(K) \end{aligned} \quad (3)$$

Thus, the rate of strength degradation depends only on the strength, the crack velocity and the materials parameter K_{IC}. Expressing the crack velocity as a simple power function of the stress intensity factor

$$V = AK_I^n = AK_{IC}^n(\sigma/S)^n \quad (4)$$

the rate of strength decrease becomes

$$dS/dt = -(AY^2K_{IC}^{n-2}/2)(\sigma/S)^nS^3 \quad (5)$$

This equation gives the slope of the strength degradation curve at any point on the strength degradation diagram (Fig. 2). Provided appropriate values of A and n are used, Equation 5 is applicable to each region of behaviour in multi-region crack growth exposure. As will be shown below, this finding has important implications in determining the minimum strength of a set of components that have been proof-tested. For a given value of σ/S, the rate of strength degradation, $-dS/dt$, increases as n increases. Note that when $n = 0$ (region II crack growth) dS/dt decreases in absolute magnitude as the strength decreases, equaling zero as S approaches zero. Consequently, dS/dt exhibits

*As is shown in Equation 3, the slope of the strength curve depends on both the crack length and the crack velocity. Since both of these are continuous throughout the test region, the slope must be continuous.

positive curvature when $n = 0$.* For region I ($n \geqslant 15$) or for region III ($n \geqslant 100$) crack growth, however, dS/dt exhibits strong negative curvature.

For any load cycle, Equation 5 can be integrated analytically to provide a relation between the initial strength, S_i (i.e. before proof testing), and the strength, S at any time, t, during the proof test cycle.

$$S^{n-2} - S_i^{n-2} = -(1/B)\int_0^t \sigma(t)^n dt, \quad (6)$$

where $(1/B) = (n-2)AY^2K_{IC}^{n-2}/2$. The amount of strength degradation during a stress cycle depends only on the integral given on the right hand side of the equation, so that the strength degradation can be determined for any stress cycle provided the applied stress, σ, is known as a function of time [6].

For a typical proof test, a component is loaded at a constant loading rate, $\dot{\sigma}_1$, held at the proof load, σ_p, for a time t_p, and then unloaded at a constant rate, $\dot{\sigma}_u$. The times for loading, t_1, and unloading, t_u, the specimens are given by $t_1 = \sigma_p/\dot{\sigma}_1$ and $t_u = \sigma_p/\dot{\sigma}_u$. Integrating Equation 6 for a typical load cycle then gives the following equation for the final strength, S_f [7]

$$S_f^{n-2} = S_i^{n-2} - (1/B)[\sigma_p^n t_p + \sigma_p^{n+1}(1/\dot{\sigma}_1 + 1/\dot{\sigma}_u)/(n+1)] \quad (7)$$

for any component that does not break during the proof test.

The development of adequate proof testing procedures for ceramic materials requires the strength distribution after proof testing to be well characterized, especially in the low strength regime. This characterization is especially necessary when fracture and/or crack propagation occurs during the unloading cycle of the proof test. To characterize fully the strength distribution after proof testing it is necessary not only to know S_f (Equation 7), but also to know the breaking stress of those specimens that fail during the proof test. This step is needed for the determination of the minimum survival strength after the proof test.

The breaking stress, σ_*, of those that fail during the unloading portion of the proof test can be obtained from Equation 6 by setting $S = \sigma_*$. The upper limit of integration of Equation 6 is then equal to $t = \sigma_p/\dot{\sigma}_1 + t_p + (\sigma_p - \sigma_*)/\dot{\sigma}_u$, which is the total time to failure during the proof test. The equation so obtained is given by

$$\sigma_*^{n-2} - (1/B)\sigma_*^{n+1}/(n+1)\dot{\sigma}_u = S_i^{n-2} - (1/B)[\sigma_p^n t_p + \sigma_p^{n+1}(1/\dot{\sigma}_1 + 1/\dot{\sigma}_u)/(n+1)]. \quad (8)$$

There are now two equations i.e. Equations 7 and 8, that describe specimen behaviour during a

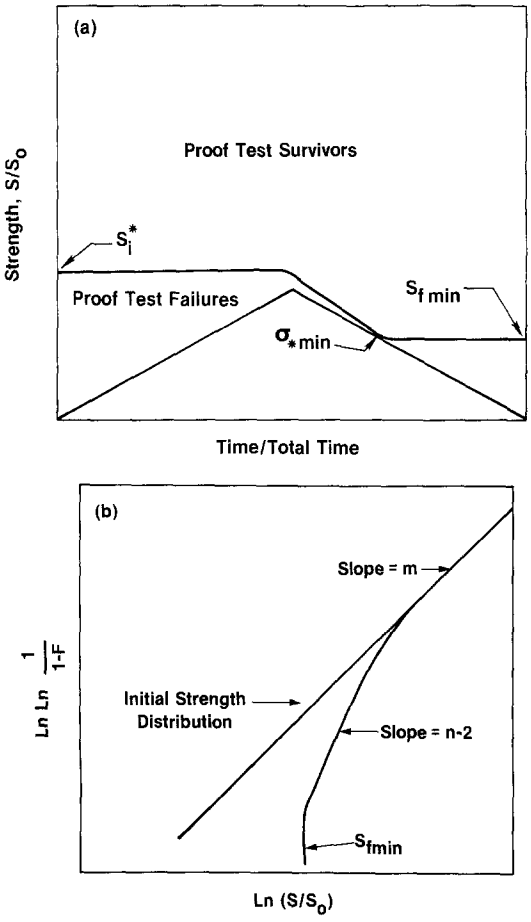

Figure 3 Single region crack propagation. (a) Definition of critical initial strength, S_i^*, minimum failure stress, σ_{*min}, and minimum strength, S_{fmin}, after the proof test. Specimens with initial strengths greater than S_i^* will survive, while those with strengths less than S_i^* will fail. Equal loading and unloading rates during the proof test are assumed in this diagram. (b) Theoretical strength distribution after proof testing. The curve is a graphical representation of Equation 18. As discussed in the text, the truncation strength depends only on the rate of unloading, $\dot{\sigma}_u$, the critical stress intensity factor, K_{IC} and the crack propagation parameters, n and A.

*Note, this conclusion holds for all $n < 3$.

proof test. Equation 7 gives the strength, S_f, of components that pass the proof test cycle, whereas Equation 8 gives the breaking stress, σ_*, of components that do not pass the proof test cycle. Both equations are expressed in terms of the load cycle parameters (σ_p, $\dot{\sigma}_1$, $\dot{\sigma}_u$, t_p), the crack propagation parameters (B and n) and the initial component strength, S_i, before the start of the proof test cycle. If the initial strength, S_i, is relatively high, the component will pass the proof test; whereas if the initial strength is low, the component will break during the proof test cycle (Fig. 3a). There is a critical initial strength, S_i^*, that will separate components that break, $S_i < S_i^*$, from those that survive, $S_i > S_i^*$, the proof test cycle. The component that has an initial strength that is infinitesimally greater than S_i^* will have a final strength, S_{fmin}, that forms a lower bound for the strengths of components that pass the proof test (Fig. 3a). S_{fmin} is important because it represents the lowest possible strength of components that have been subjected to a proof test cycle. S_{fmin} is in effect the truncation strength for the strength distribution after the completion of the proof test. By similar reasoning, the component that has an initial strength that is infinitesimally less than S_i^* will break at a stress, σ_{*min}, that forms a lower limit to the breaking stresses of components that fail during the unloading cycle (Fig. 3a).

A relationship between the minimum strength, S_{fmin}, after the proof test cycle, and the minimum breaking stress, σ_{*min}, can be obtained by setting $S_i = S_i^*$ in Equations 7 and 8 and equating the left-hand sides of these equations

$$S_{fmin}^{n-2} = \sigma_{*min}^{n-2}[1 - (1/B(n+1))(\sigma_{*min}^3/\dot{\sigma}_u)]. \quad (9)$$

Equation 9 can be simplified by expressing σ_{*min} in terms of the unloading rate. During unloading, the strength degradation curve that characterizes S_{fmin} will approach within an infinitesimally small distance of the stress curve, but will fail to touch it. At the point of closest approach of the two curves, the slope, dS/dt, of the strength curve will be equal to the slope, $-\dot{\sigma}_u$, of the stress curve. By letting $dS/dt = -\dot{\sigma}_u$ and $\sigma = S = \sigma_{*min}$ in Equation 5, the following equation is obtained

$$\sigma_{*min} = [B(n-2)\dot{\sigma}_u]^{1/3}. \quad (10)$$

By substituting this relation for $\dot{\sigma}_u$ in Equation 9 a simple equation is obtained for the minimum strength after proof testing

$$S_{fmin} = \sigma_{*min}[3/(n+1)]^{1/(n-2)}. \quad (11)$$

One concludes from this equation that the strength, S_{fmin}, of a component that just survives the proof test is always less than the breaking stress, σ_{*min}, of one that just breaks during the proof test. Because n for most ceramic materials is large, > 10, S_{fmin}/σ_{*min} is normally greater than 0.85.

Equation 10 can be written in an alternative form that is useful when relating the truncation strength, S_{fmin}, to parameters that describe crack growth. By expressing B in terms of the crack growth parameters A and n, and by defining a limit crack velocity (Fig. 1b), $V_{IC} = AK_{IC}^n$, the following alternative representation of Equation 10 is obtained

$$\sigma_{*min} = [(2\dot{\sigma}_u K_{IC}^2)/(V_{IC} Y^2)]^{1/3}. \quad (12)$$

From Equations 11 and 12 we note that the truncation strength, S_{fmin}, depends only on the unloading rate, $\dot{\sigma}_u$, the critical stress intensity factor, and the limit crack velocity, V_{IC}, which is determined by the crack propagation parameters, A and n. Therefore, the truncation strength does not depend on the proof test level, the time at load, or the loading rate. If $\dot{\sigma}_u > 0$, Equations 11 and 12 imply that proof testing always truncates the strength distribution. The higher the unloading rate, $\dot{\sigma}_u$, the greater is the strength level, S_{fmin}, at which strength truncation occurs. Fracture during the unloading part of the cycle can be avoided provided the unloading rate is sufficiently great that σ_{*min} calculated from Equations 10 or 12 is greater than the proof test load, σ_p. This condition for truncation was noted earlier by Evans and Fuller [7] from other considerations. However, even if $\sigma_{*min} \geqslant \sigma_m$, strength degradation will still occur during unloading so that S_{fmin} will be less than σ_p (Equation 11). Finally, since the only crack growth parameters that influence σ_{*min} are those that occur when $V = V_{IC}$, Equation 12 should also apply to multi-region crack growth, for which the intersection of the region III curve with K_{IC} (Fig. 1b) normally determines V_{IC}.

4. Single region crack propagation: statistical parameters

Since proof testing modifies the initial strength distribution, a discussion of the shape of the distribution curve that results from proof testing is important. The treatment of strength degradation

given above provides all of the necessary information to determine the effect of a stress cycle on the strength distribution. The change in strength during the proof test can be determined from Equation 7, while the change in probability can be determined from simple probability theory. Therefore, if the inital strength, S_i, is known as a function of the initial cumulative failure probability, F_i, the strength after proof testing, S_f, can be evaluated in terms of the cumulative failure probability, F_f, of the components that pass the proof test by the use of simple transformations of both strength (Equation 7) and failure probability. This approach to estimating the effect of proof testing on the strength distribution is illustrated below for a two-parameter Weibull distribution. Although the approach is not limited to Weibull statistics, this form of extreme value statistics is easy to use and provides a relatively accurate description of the strength distribution for brittle materials. Two parameter Weibull statistics can be easily incorporated into the present treatment of proof testing, so that strength distributions after proof testing can be expressed in terms of statistical parameters [3, 7, 10, 11].

Weibull statistics relate the cumulative failure probability, F, to the strength, S, by the following standard equation* [12]

$$\ln(\ln(1-F)^{-1}) = m \ln(S/S_o), \quad (13)$$

where m and S_o are parameters that are determined from experimental data by a least-squares fit or by other methods of estimation [13]. For simplicity in succeeding calculations let $\ln(1-F)^{-1} \equiv Q$. Note that for small values of the failure probability $Q = F$ ($F < 0.01$). If Q_i is determined by the initial strength distribution before proof testing, then Equation 13 can be simply expressed as

$$Q_i = (S_i/S_o)^m. \quad (14)$$

From probability theory the initial failure probability (as characterized by Q_i) can be related to the failure probability after proof testing (as characterized by Q_f) and the failure probability of the component that just fails during the proof test (characterized by Q_p).†

$$Q_i = Q_f + Q_p. \quad (15)$$

By substituting Equations 14 and 15 into Equation 7, the strength S_f, after a proof test can be expressed in terms of the cumulative failure probability (represented by Q_f)

$$(S_f/S_o)^{n-2} = (Q_f + Q_p)^{\frac{n-2}{m}} - (1/B)S_o^{-(n-2)} \times [\sigma_p^n t_p + \sigma_p^{n+1}(1/\dot{\sigma}_1 + 1/\dot{\sigma}_u)/(n+1)]. \quad (16)$$

Equation 16 can be simplified considerably by noting that for the specimen that just survives the proof test cycle $S_f \to S_{fmin}$ and $Q_f \to 0$. Substituting for S_f and Q_f in Equation 16, the following expression is obtained for the last term on the right of Equation 16

$$(1/B)S_o^{-(n-2)}[\sigma_p^n t_p + \sigma_p^{n+1}(1/\dot{\sigma}_1 + 1/\dot{\sigma}_u)/(n+1)] = Q_p^{\frac{n-2}{m}} - (S_{fmin}/S_o)^{n-2}. \quad (17)$$

Substituting this expression into Equation 16 eliminates the term contained in the square bracket so that

$$(S_f/S_o)^{n-2} = (Q_f + Q_p)^{\frac{n-2}{m}} - Q_p^{\frac{n-2}{m}} + (S_{fmin}/S_o)^{n-2}. \quad (18)$$

Equation 18 illustrates the important conclusion that once S_{fmin}, S_o, m and n are determined the strength distribution after a proof test can be determined simply by counting the number of specimens that break during the proof test.‡

For single region crack growth, Equation 18 gives a complete description of the type of probability curve expected for the strength distribution after proof testing. It is straightforward to show that the strength distribution after proof testing is given by a trimodal curve, each part of which corresponds to a different range of initial strengths

*F is obtained by ordering a set of strength data. F is given by $r/(N+1)$ where N is the total number of datum points and r is the position of each point in the ordered set. $r = 1$ for the lowest strength value, $r = 2$ for the second lowest and so forth.

†Equation 15 follows from the probability relation $F_f = (F_i - F_p)/(1 - F_p)$ where F_f is the failure probability after proof testing, F_i is the initial failure probability evaluated from Equation 13 and F_p is the proof test failure probability [10].

‡S_{fmin} approaches zero as the unloading rate becomes vanishingly small (Type III distribution [7] discussed in part I of this paper), and has an upper limit when $S_{fmin} = \sigma_p$ (i.e. infinite unloading rate, for which no crack growth occurs during the proof test, Type II distribution [7, 10] discussed in part 1 of this paper.)

and corresponding failure probability (Fig. 3b). When strengths before testing are high, little crack growth occurs during the proof test, and as a consequence, strength degradation resulting from the proof test is slight (Fig. 2). In quantitative terms, the strength after the proof test will be much greater than the proof test stress ($S_f \gg \sigma_p$), so that $Q_f \gg Q_p$. If the final strength is also much larger than the truncation strength ($S_f \gg S_{fmin}$), then the strength distribution after the proof test (calculated from Equation 18) is given by $(S_f/S_o)^m = Q_f$, which is identical to the initial distribution (Equation 14). This portion of the strength distribution is indicated by a slope of m in Fig. 3b.

For an intermediate range of initial cummulative failure probabilities, strength degradation resulting from crack growth significantly alters the strength distribution after proof testing. If the final strength is significantly greater than the truncation strength ($S_f \gg S_{fmin}$), and if the failure probability after proof testing, Q_f, is less than the failure probability, Q_p, calculated from $Q_p = (\sigma_p/S_o)^m$ (i.e. $Q_f \ll Q_p$), then the strength distribution given by Equation 18 can be simplified by expanding $(Q_f + Q_p)^{(n-2)/m}$ as a Taylor series. The final distribution for the intermediate probability range is then given by

$$Q_f = [m/(n-2)]\,Q_p^{(m+2-n)/m}(S_f/S_o)^{(n-2)}, \tag{19}$$

which implies that the strength distribution after proof testing can be represented by a straight line with a slope $m' = n - 2$ (Fig. 3b). Finally, in the lowest probability range, the strength distribution must be truncated so that $S_f = S_{fmin}$, where S_{fmin} is given by Equation 11.

In summary, the strength distribution after proof testing can be described by two Weibull curves (Fig. 3b): one at higher probabilities having a slope of m; the other at lower probabilities having a slope of $n - 2$. As indicated in Fig. 3b, the low probability curve is truncated at a strength given by S_{fmin}.

5. Single region crack propagation: examples of strength degradation maps and Weibull diagrams

The equations presented in the previous sections will now be illustrated for the special case of single-region crack propagation in soda-lime–silica glass. Experimentally determined values of A and n were selected to represent crack propagation in air (50% r.h.) and dry nitrogen gas (~ 0% r.h.). To illustrate the effect of unloading rate on strength, two values (1 MPa sec^{-1} and 1000 MPa sec^{-1}) were used for each environment, the loading rate was conveniently set equal to the unloading rate and the hold time was set equal to zero. The strength/stress axes of the resulting strength degradation maps shown in Figs. 4 and 5 are represented in terms of the reduced variables S/S_o and σ/S_o, where S is the strength, σ is the stress and S_o is the Weibull strength measured in an inert environment. The time axes in these figures are plotted in terms of the reduced variable t/T where T is the total time of the proof test cycle.

Figs. 4a and b illustrate the predicted effect of moist air (50% r.h.) on the strength of soda-lime–silica glass specimens for the loading conditions just specified. The strength degradation map for a loading rate of 1 MPa sec^{-1} (Fig. 4a) illustrates a number of features discussed in the previous sections: at high initial strengths relatively little strength degradation occurs during the stress cycle; at low initial strengths, the strength decreases relatively rapidly once the stress reaches a sizable fraction of the initial strength. Over a relatively narrow range of initial strengths that separate those specimens that fail from those that survive the proof test, a dramatic change in the shape of the strength degradation curve is observed. The strength curve bends over as the unloading cycle begins, and the strength appears to decrease at a relatively constant rate as the stress is decreased further. Specimens with initial strengths that are just above the critical value survive the proof cycle; initial strengths that are just below critical fail the proof cycle. Note that significant strength degradation occurs for specimens that just pass the proof test and that a significant number of failures can occur during the unloading portion of the proof test cycle. The truncation strength for conditions given for Fig. 4a was $S_{fmin} = 0.035\,S_o$.

The effect of higher loading rates on strength is shown in Fig. 4b. As can be seen from this figure increasing the loading rate to 1000 MPa sec^{-1} decreases the value of S_i that just survives fracture. Also, the value of the truncation stress $S_{fmin} = 0.35\,S_o$ is increased by one order of magnitude as the loading rate is increased by three orders of magnitude. For tests in dry nitrogen (Figs. 4c and d) strength degradation curves are similar to those

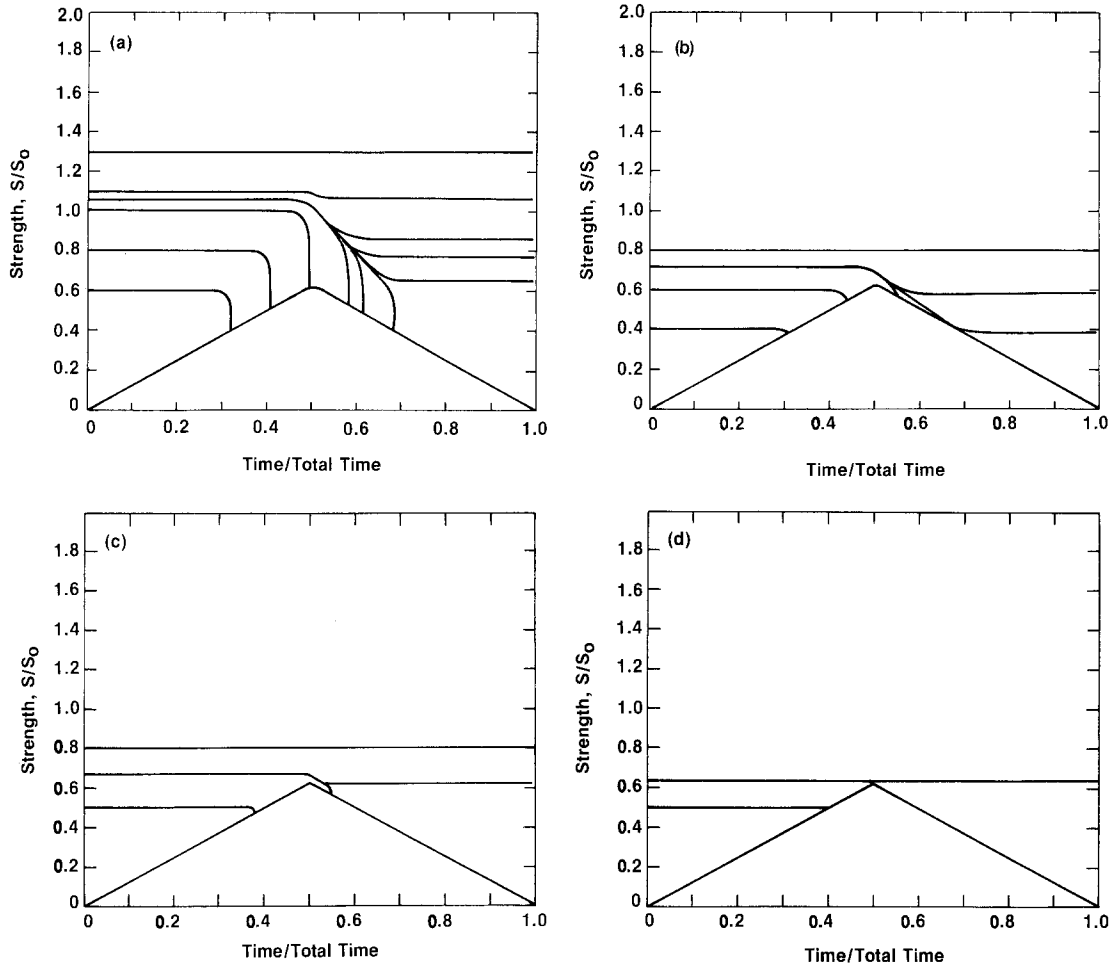

Figure 4 Region I crack growth: schematic diagrams of strength degradation maps for soda-lime–silica glass. (a) loading rate: 1 MPa sec^{-1}. Test in air; 50% r.h. ($n = 19.7$, $\ln A = -271.9$) (b) loading rate: 1000 MPa sec^{-1}. Test in air, 50% r.h. (c) loading rate: 1 MPa sec^{-1}. Test in dry air, 0.01% r.h. ($n = 120.9$, $\ln A = -1641.4$) (d) loading rate: 1000 MPa sec^{-1} dry air, 0.01% r.h. $m = 7.7$; $S_o = 126.9$ MPa; $K_o = 0$ MPa-$m^{1/2}$; $K_{IC} = 0.75$ MPa-$m^{1/2}$, $\sigma_p = 0.65\ S_o$.

just discussed, however because water is not present, strength degradation is less for all levels of initial strength, and far fewer components break during the proof test.

Fig. 5 illustrates the effect of environment and loading rate on the strength distribution after proof testing. For all test conditions, the curves obtained for specimens that survive the proof test approaches the curve that represents the initial strength distribution (the straight lines in Fig. 5). At low probability levels the curves for the proof test survivors approach a slope of $n - 2$, as expected. For the test conditions selected, the truncation strength occurs at a value too low to be represented on Fig. 5. The effect of loading rate on the strength distribution after proofing can be discerned by comparing Figs. 5a and b for the moist environment. Because far fewer specimens break at the high loading in the moist environment, (~ 7 per cent for 1000 MPa sec^{-1} against ~ 78 per cent for 1 MPa sec^{-1}), the low probability portion of the survival curve shown in Fig. 5b has shifted to lower strength values relative to the curve in Fig. 5a. This effect of loading rate on the survival curve is greatly suppressed in dry environments, as can be discerned by the fact that virtually the same survival curve is obtained at low and high loading rates (Figs. 5c and d). For the same loading conditions, proof testing in dry environments greatly reduces the number of failures during the proof test (~ 2.9 per cent at 1000 MPa sec^{-1} and ~ 4.5 per cent at 1 MPa sec^{-1}). Furthermore since the slope of the survival curve increases at low failure probabilities, the probability of failure at a given strength after proof testing is greatly reduced by

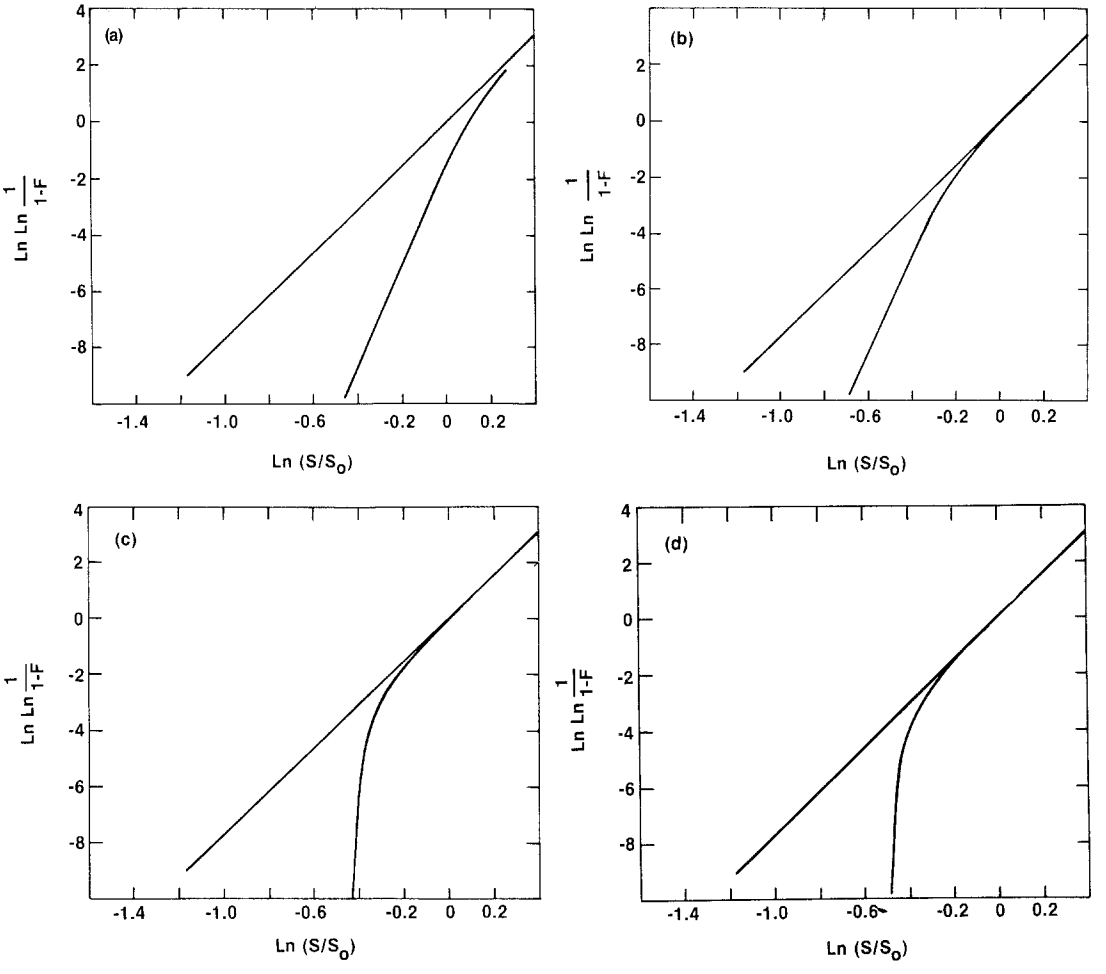

Figure 5 Region 1 crack growth: schematic diagram of strength distribution after proof testing for soda-lime–silica glass. (a) loading rate 1 MPa sec^{-1}. Test in Air, 50% r.h. (b) loading rate 1000 MPa sec^{-1}. Test in air 50% r.h. (c) loading rate 1 MPa sec^{-1}. Test in Air 0.01% r.h. (d) loading rate 1000 MPa sec^{-1}. Test in air 0.01% r.h. (Experimental constants constants used for this figure are given in Fig. 4.)

using a dry environment for the proof test, thus confirming the importance of environmental control during proof testing.

6. Multi-region behaviour: examples of strength degradation maps and Weibull diagrams

Multi-region crack propagation can, in principle, be handled by the same mathematical techniques discussed in Sections 2 and 3. Equation 7 would be applicable within each region of crack growth, with appropriate values of A and n being used to describe crack growth behaviour. As the strength degradation curve passes between two regions of crack growths, boundary conditions require that both the strength and the slope of the strength degradation curve (dS/dt) be continuous. Given the initial strength, Equation 6 can be used to estimate either the final strength (if the strength curve does not intersect the boundary line between Region I and II), or the strength at the intersection of the boundary. Determination of the strength at the intersection with the boundary requires an interative procedure to be applied to Equation 6 because both the limits of integration of Equation 6 and the strength depend on the point of intersection of the strength curve with the boundary. Once the strength at the boundary is determined, this same procedure can be repeated to estimate the strength at other boundaries of the strength degradation map. It is worth emphasizing that, depending on the initial strength, a strength degradation curve can either exit from a region of crack growth by going to the next region (i.e.,

Region II to Region III), or by going back to the previous region of crack growth, (i.e., Region II to Region I). Because of these complexities, strength degradation maps are obtained more easily by direct numerical integration of crack propagation data.

The computer routine used here to investigate multi-region crack propagation is based on a direct integration of Equation 3, assuming that the rate of crack growth is controlled by Equation 4. Given an initial strength, the crack length can be determined from Equation 2. The stress for crack growth determined from the stress cycle is then used to calculate the crack velocity from Equation 4. For a time increment, dt, the change in crack length, da, during dt is determined from the crack velocity, $da = v dt$. Finally a new length, $a + da$, is used to calculate a new strength, which completes one iteration of the computer cycle. By repeating the calculation many times, the rate of change of strength with time can be determined. At the end of each cycle, a comparison is made between the calculated strength and boundary-value conditions (see Fig. 2b) to determine the appropriate crack growth parameters that are applicable (i.e., the correct region of crack growth). If the condition $S = \sigma$, is attained fracture is assumed to occur. This numerical method was used as a subroutine in a larger program to obtain strength degradation maps, Weibull diagrams, and strength histograms. These diagrams demonstrate the effects of multi-region crack propagation on the strength of materials. As will be shown in a comparison of multi-region maps with their counterparts described in Fig. 4, Region II crack growth behaviour has a significant effect on the appearance of these diagrams.

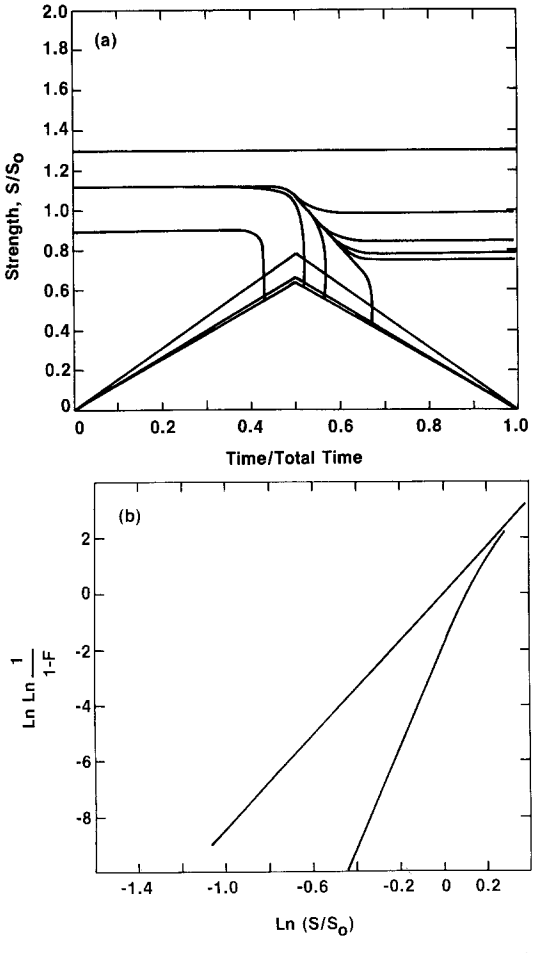

Figure 6 Multi-region crack growth: Air 50% r.h., loading rate: 1 MPa sec^{-1} (a) strength degradation map. (b) Strength distribution after proof test. Crack growth parameters for Fig. 6 to 9: Region I, $n = 19.7$, $\ln A = -271.9$; Region II, $v = 1 \times 10^{-4}$ m sec^{-1}; Region III, $n = 120.9$, $\ln A = -1641.4$. Weibull parameters for figures 6 through 9: $S_o = 137.9$ MPa, $m = 8.4$. Other constants for Fig. 6 to 9: $K_{IC} = 0.75$ MPa-$m^{1/2}$; $K_o = 0$ MPa-$m^{1/2}$; $\sigma_p = 0.65\, S_o$.

The main features of strength degradation in a moist environment (air, 50 per cent r.h.) are shown in Figs. 6 to 8. When specimens are loaded and unloaded relatively slowly (1 MPa sec^{-1}), both the strength degradation map (Fig. 6a) and the Weibull plot (Fig. 6b) look similar to those obtained for single mode propagation in moist nitrogen gas, (50 per cent r.h., Figs. 4a and 5a) By contrast, at high loading rates (1000 MPa sec^{-1}), the strength degradation map (Fig. 7a) and the Weibull diagram (Fig. 7b) are nearly identical to those obtained for single mode propagation in dry nitrogen. Thus, the distribution after proof testing seems to be determined mainly by Region I crack growth when the rate of loading is slow, and by Region III crack growth when the rate of loading is high.

At intermediate loading rates, Region II crack growth behaviour dominates the shape of the strength distribution curves of specimens that survive the proof test cycle. As illustrated in Fig. 8a, the effect is most pronounced when the slope of the strength degradation curve is slightly greater than the slope of the line that represent the boundary between Region I and Region II crack propagation. From Equation 5, we see that once the strength curve enters Region II, its curvature changes from negative (large n) to positive ($n = 0$), so that the slope decreases as S decreases, with the consequence that components with a range of initial strengths that normally

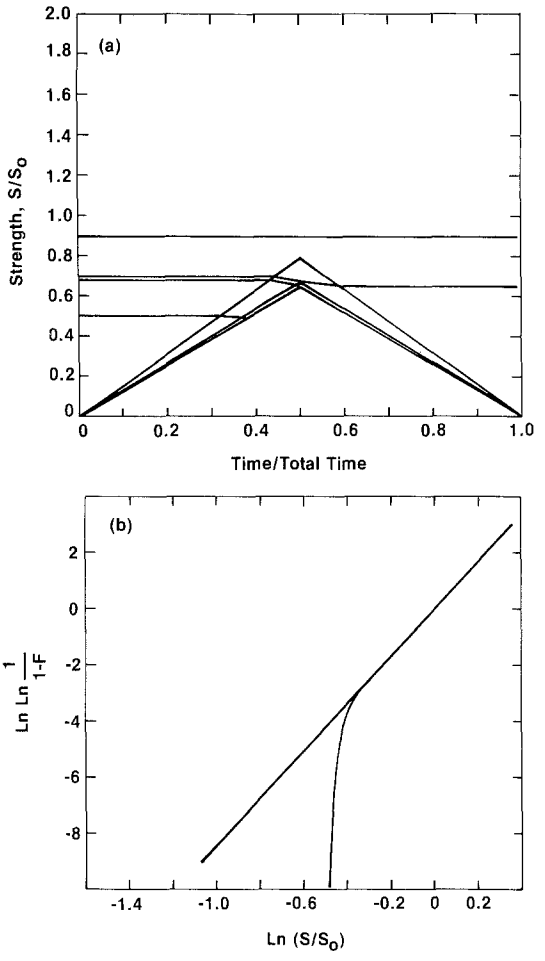

Figure 7 Multi-region crack growth: Air 50% r.h., loading rate: 1000 MPa sec^{-1} (a) Strength degradation map. (b) Strength distribution after proof testing.

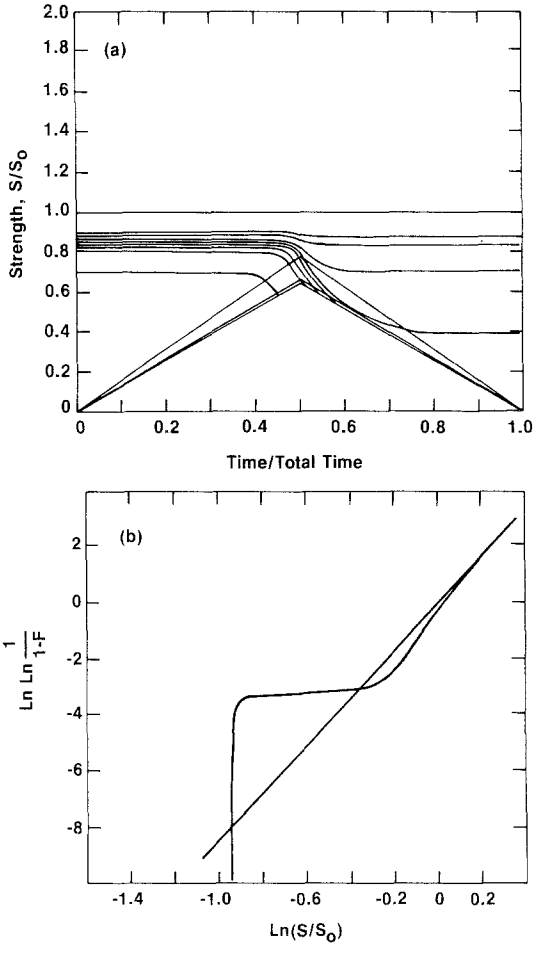

Figure 8 Multi-region crack growth: Air 50% r.h., loading rate: 100 MPa sec^{-1} (a) strength degradation map; (b) strength distribution after proof testing.

would have failed during the load cycle (for single region crack growth) now survive, but with a greatly reduced strength. Because of this behaviour, the Weibull curves (Fig. 8b) are severely distorted. Instead of consisting of two straight lines with a truncation stress at low probabilities (Fig. 3b), the Weibull curve exhibits a large plateau which indicates a constant cumulative failure probability for a fairly wide range of final strengths, S_f. Therefore, the probability of finding specimens with strengths that lie within the strength range of the plateau is small. This plateau in the Weibull curve suggests a bimodal strength distribution with a small peak in the distribution at low levels of strength. This type of distribution is potentially dangerous for materials that are intended for structural applications.

The shape and position of the plateau shown in Fig. 8b, is affected by both the stress cycle parameters and the crack propagation parameters. Although the probability level of the plateau is found to vary as σ_p is changed; the truncation strength is unaffected by σ_p, provided the stressing rate remains constant (Fig. 9). This result is consistent with the discussion in Section 2 and with Equations 10 and 12, which are also applicable to multi-region crack growth. Increasing the stressing rate almost completely eliminates the effect of Region II crack propagation (Fig. 7b). Conversely, decreasing the stressing rate suppresses the plateau to low probability levels (so that it does not appear in the diagram). The effect of Region II crack propagation on the strength distribution is enhanced as the width of Region II is increased. Here, the main effect of Region II crack growth on the Weibull curve is to increase the range of stresses over which the plateau occurs.

With regard to proof testing as a method of

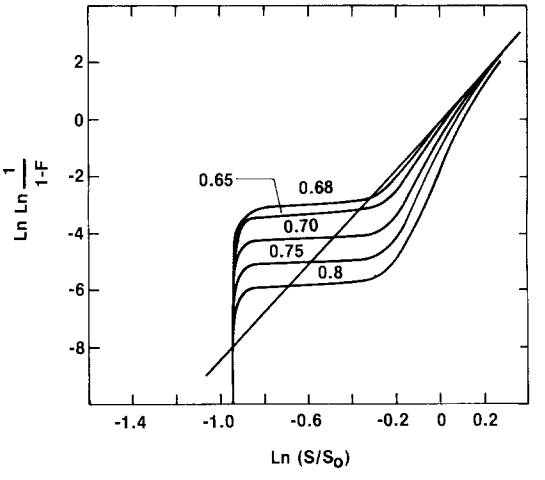

Figure 9 Dependence of strength distribution after proof test on proof test stress, σ_p, indicated by the numbers associated with each curve. Loading rate: 100 MPa sec^{-1} Air, 50% r.h.

assuring component reliability, a disturbing aspect of Region II crack propagation is that, for equivalent failure probabilities, portions of the strength distribution after proof testing lie at lower strength levels than those given by the initial distribution, resulting in significant probabilities of failure at low stresses after proof testing. This effect occurs for both dry test environments (Fig. 10) and moist test environments (Fig. 8b). The effect can result in either a significant strength degradation or an apparently unchanged strength distribution as a result of the proof test (high probability region of Fig. 8b). Effects such as these have been reported in Part I of this study and have a plausable explanation in terms of Region II crack propagation. For practical purposes, elimination of these effects can be accomplished most easily by increasing the rate of unloading during a proof test. Thus, even for a relatively moist environment, rapid unloading (Fig. 7b) leads to a distribution after proof testing that is sharply truncated and is better than the initial distribution at all probability levels. Equation 10, with $\sigma_{*min} = \sigma_p$, provides a quantitative estimate of the unloading rate needed for effective truncation of the strength distribution curve in a moist environment such as air [7].

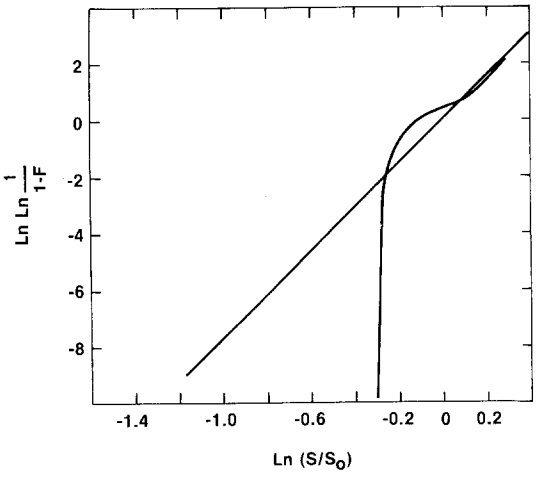

Figure 10 Strength distribution after proof test: air 0.01% r.h.; loading rate, 1 MPa sec^{-1}; $\sigma_p = 0.82\ S_o$. Crack growth parameters: Region I, $n = 19.7$, $\ln A = -276.5$; Region II, $v = 1.5 \times 10^{-7}$ m sec^{-1}; Region III, $n = 120.9$, $\ln A = -1641.4$. Weibull parameters: $S_o = 126.9$ MPa sec^{-1}; $m = 7.7$.

As a final comment, referring to the discussion at the end of Part I of this paper, it is noted that the theory presented in this part provides the basis for understanding strength degradation of ceramic materials. The theory has been used in Part I to explain the general shape of strength distribution resulting from proof testing. The fact that detailed agreeement between theory and some experiments was not obtained suggests that our understanding of subcritical crack growth in specimens that contain small cracks (e.g. $< 10\,\mu$m) is not complete, and requires further research. The discussions presented in this part of the paper should help in interpreting any new data.

Acknowledgements

Two of the authors (E. R. Fuller, Jr and S. M. Wiederhorn) are grateful for the support of the Department of Energy, Fossil Fuel Utilization Division; the others (J. E. Ritter, Jr and P. B. Oates) are grateful for the support of the National Science Foundation, contract DMR-77-05647.

References

1. S. M. WIEDERHORN "Fracture Mechanics of Ceramics" Vol. 4, edited by R. C. Bradt, D. P. H. Hasselman and F. F. Lange (Plenum Publishing Co., New York, 1978) pp. 549-80.
2. *Idem, ibid.* Vol. 2, edited by R. C. Bradt, D. P. H. Hasselman and F. F. Lange (Plenum Publishing Co., New York 1974) pp. 613-46.
3. JOHN E. RITTER, Jr. "Fracture Mechanics of Ceramics" Vol. 4, edited by R. C. Bradt, D. P. H. Hasselman and F. F. Lange (Plenum Publishing Co., New York, 1978) pp. 667-86.
4. S. M. WIEDERHORN, *J. Amer. Ceram. Soc.* **50**, (1967) 407.
5. A. G. EVANS, *J. Amer. Ceram. Soc.* 57 (1974) 410.

6. A. G. EVANS and E. R. FULLER, *Met. Trans.* **5** (1974) 27.
7. *Idem, Mater. Sci. and Eng.* **19** (1975) 69.
8. A. G. EVANS and H. JOHNSON, *J. Mater. Sci.* **10** (1975) 214.
9. A. G. EVANS, *Inst. J. Fract.* **10** (1974) 251.
10. A. G. EVANS and S. M. WIEDERHORN, *ibid.* **10** (1974) 379.
11. S. M. WIEDERHORN, "Reliability, Life Prediction and Proof Testing of Ceramics: High-Performance Applications" edited by J. J. Burke, A. E. Gorum and R. N. Katz (Brook Hill Publishing Co., Chestnut Hill, Mass., 1974) p. 635.
12. W. WEIBULL, *J. Appl. Mech.* **19** (1951) 293.
13. N. R. MANN, R. E. SHAFER and N. D. SINGPURWALLEE "Methods for Statistical Analysis of Reliability and Life Data" (John Wiley & Sons, New York, 1974).

Received 14 November 1970 and accepted 5 February 1980.